ORIGINAL PAPER

C. C. Lin

High-pressure Raman spectroscopic study of Co- and Ni-olivines

Abstract The Raman spectra of synthetic α-Co$_2$SiO$_4$ and α-Ni$_2$SiO$_4$ olivines have been studied at room temperature and various pressures. All the Raman frequencies of the two olivines increase with increasing pressure, and most of the frequency–pressure plots obtained under both quasi- and nonhydrostatic conditions are nonlinear. It has been found that the average pressure derivative of Raman frequencies of the lattice modes in both Co- and Ni-olivines is smaller than that of the internal modes of SiO$_4$, indicating that the distortion of SiO$_4$ tetrahedra under static compression may be more severe than that of MO$_6$ octahedra. In addition, four new Raman bands were observed in Ni-olivine under nonhydrostatic compression and above 30 GPa. This result suggests that a new phase of Ni-olivine should be formed at 30 GPa or amorphization may occur at still higher pressure.

Key words Transition metal olivines · Raman spectroscopy · High pressure

Introduction

Study of the properties of olivines is an attractive subject in mineralogy and Earth sciences because these minerals are believed to be a dominant phase in the Earth's upper mantle. As a result, a number of studies have been carried out to explore the effect of pressure on the physical properties of the forsterite–fayalite system. However, naturally occurring ferromagnesian olivines always contain minor amount of other divalent cations, particularly Ca^{2+}, Mn^{2+} (usually in Fe-rich olivines), and Ni^{2+} (usually in Mg-rich olivines) (Brown 1982; Deer et al. 1992). This fact suggests that the possible influences from other cations should not be neglected if we want to understand the exact properties of olivine under mantle conditions.

By substitution of the divalent transition metal cations for Mg^{2+}, it has been found that the pressure for the olivine to spinel ($\alpha \rightarrow \gamma$) transition is significantly lowered (Syono et al. 1971). This phenomenon has been correlated with the crystal-field stabilization energy (CFSE) in the cation octahedra of the transition metal olivines. Previous study on the transition metal olivines has revealed a relationship between ambient Raman frequency of the lattice modes and both radius and CFSE of cation (Lin 2001). Therefore, investigation of the possible effect of the transition metal cations on the compressional behavior of olivine is also of mineralogical interest, and the information extracted from such a study may contribute to a better understanding of the role of transition-metal-bearing forsterite in the Earth's interior.

In addition to using X-ray diffraction, the compressional behavior of the forsterite–fayalite system has been widely studied by means of Raman spectroscopy (e.g. Hazen 1976; Besson et al. 1982; Chopelas 1990; Guyot and Reynard 1992; Sharma et al. 1992; Durben et al. 1993; Liu and Mernagh 1993; Wang et al. 1993). However, only a few Raman spectroscopic studies have been carried out on tephroite, calcio-olivine, and Ni-olivine (Sharma et al. 1992; Wang et al. 1992; Reynard et al. 1997), and no study was carried out for Co-olivine. Besides, the pressure dependence of Raman frequency for Ni-olivine was not given in previous work (Sharma et al. 1992). A study on the consistency between diffraction and Raman data is significant for the interpretation of the compressional behavior of a polyhedron in olivines. Therefore, a Raman spectroscopic study for both Co- and Ni-olivines was carried out in this work, and a comparison with forsterite was examined.

Pressure-induced amorphization has been observed in olivines that were quenched from high pressure, e.g.,

C. C. Lin
Institute of Earth Sciences, Academia Sinica,
Nankang, Taipei, Taiwan, ROC
Tel.: 886-2-2783 9910; Fax: 886-2-2783 9871
e-mail: cclin@earth.sinica.edu.tw

< 700 °C and 30 GPa for forsterite, and 35–39 GPa and room temperature for fayalite (Jeanloz et al. 1977; Richard and Richet 1990; Guyot and Reynard 1992; Williams et al. 1990). The low-temperature amorphization of olivines may be related to the formation of Si_2O_7 defect (Durben et al. 1993), and can be promoted by shear stress (Reynard et al. 1997; Richet and Gillet 1997). The criterion for such a cold melting is that the extension of melting curve in the stability field of the high-pressure phase has a negative pressure–temperature (P–T) slope (Brazhkin and Lyapin 1996; Richet and Gillet 1997). Similarly to forsterite and fayalite, both Co- and Ni-olivines also transform into the spinel phase under compression (Liu and Bassett 1986). Therefore, a nonhydrostatic compression was also carried out to estimate the possibility of amorphization of Co- and Ni-olivines at room temperature, though we do not know if the P–T slope of the extrapolation of the melting curve is negative.

Experimental

The mixtures of SiO_2, Co_3O_4, and NiO in stoichiometric ratio were used for synthesis of Co- and Ni-olivines. Powder X-ray diffraction with step scan was used to determine the phases and lattice parameters. All diffraction lines were used to calculate the parameters. The details for preparation and characterization of the samples have been described elsewhere. (Lin 2001). The synthetic samples are polycrystalline and transparent, ca. 100–200 μm in size and purple in color for Co_2SiO_4, and less than 30 μm in size and yellow-green in color for Ni_2SiO_4. The lattice parameters [based on the space group $Pbnm$ (62)] are $a = 4.790(1)$ Å, $b = 10.31(1)$ Å, and $c = 6.007(1)$ Å for Co_2SiO_4, and $a = 4.734(1)$ Å, $b = 10.133(2)$ Å, and $c = 5.922(2)$ Å for Ni_2SiO_4, where values inside the parentheses are standard deviation. These data are close to those reported in previous works (Matsui and Syono 1968; Morimoto et al. 1974).

When we conduct a high-pressure experiment by using a diamond-anvil cell, it is known that the hydrostatic condition has never been attained at a pressure above 10–15 GPa due to the development of significant unaxial stress. Among the pressure-transmitting media, helium is found to be better than argon for sustaining hydrostaticity at high pressure. However, under high pressure, it has been pointed out that helium can diffuse into forsterite crystal and hence change the anisotropy of forsterite (Downs et al. 1996). This case implies that the pressure dependences of Raman frequencies in olivines may be changed by the use of helium, though it can produce an environment with rather low nonhydrostaticity. The diffusion was not observed in the experiments using other pressure-transmitting media.

Although H_2O freezes at 0.93 GPa at room temperature, the hydrostatic behavior of ices VI and VII is about the same as an ethanol–methanol mixture at pressures below 10 GPa and is superior to the ethanol–methanol solution in the pressures above 10 GPa. The hydrostaticity of the H_2O medium at high pressures can be qualitatively estimated from the shape and separation of the R_1 and R_2 fluorescence bands of ruby. It is found that the nonhydrostaticity around a flange of crystal (analogous to the peninsula of a larger mass of land) can be kept reasonably small up to a pressure ca. 30 GPa. Therefore, the configuration of crystal should not be neglected for keeping a hydrostatic environment in the high-pressure experiment. In this work, the quasihydrostatic compression is used to denote the high-pressure experiments of collecting spectra from a flange of crystal, though the system gradually becomes nonhydrostatic with increasing pressure. In fact, the system is nearly hydrostatic below 10 GPa with the use of H_2O as pressure medium. The nonhydrostatic experiment is assigned only to the compression runs without use of a pressure-transmitting medium.

In the quasihydrostatic high-pressure experiments, one or two chips of the samples, approximately 20–40 μm in size, were placed inside the hole (150 μm in diameter and 60–80 μm in depth) in a hardened stainless steel gasket in a Mao-Bell-type diamond-anvil cell with anvil faces of approximately 600 μm in diameter. Note that the Co-olivine chips are fragments from larger crystals. All crystal chips were confirmed to be single crystals by using a polarized microscope. Fine powders of ruby were also placed inside the hole, and deionized water was used as a pressure-transmitting medium. Below 1000 cm^{-1}, the Raman bands of water and ices VI and VII are weak and broad at various pressures and room temperature. Thus, the Raman bands of the pressure medium do not interfere with the recognition of sample signals. The whole assembly was then sealed by compressing the diamond anvils. The samples were set on the top of ruby powders, and the Raman spectra of the samples and the ruby fluorescence spectrum were measured at the same spot. This procedure tends to reduce the frequency errors caused by the pressure gradient across the samples. Pressures were measured using the ruby-fluorescence technique.

For nonhydrostatic compression, no pressure-transmitting medium was used. Fine powders of ruby were first placed inside the hole of the gasket, and then overlaid by the sample crystals. The other details for the nonhydrostatic runs are the same as those described for the quasihydrostatic experiment. Based on the shape and separation of the R_1 and R_2 bands of ruby, it indicates that the sample under nonhydrostatic condition has encountered a more severe shear stress than that under quasihydrostatic condition.

The pressure variation study was carried out on a Renishaw-2000 Raman microprobe, and the backscattering (180°) spectra were obtained with the 514.5-nm line from a Coherent Innova argon ion laser. The spectra were recorded with a Leitz UM 32 microscope objective and three accumulations at 300-s integration time with ~60 mW power on the sample. The focused laser spot on the sample was estimated to be 2–4 μm in diameter. Wavenumbers are accurate to ±1cm^{-1} as determined from plasma emission lines. The frequency of each Raman band was obtained by Lorentzian curve fitting using the Jandel Scientific Peakfit computer software. It is noted that the polarization resulting from the vibration of a group of atoms is a vector. Thus, the intensity of a Raman band is related to orientation of crystal. However, the ambient Raman frequencies and intensities reported in this work for the two olivines are the averages that collected from many crystals with random distribution in the orientation of these crystals.

Results and discussion

Figure 1 shows the typical ambient Raman spectra of Co- and Ni-olivines. The ambient Raman data of the two olivines and the corresponding symmetries and assignments used in forsterite (Iishi 1978) are listed in Table 1. According to factor group analysis, a total of 36 Raman modes are predicted for olivines (e.g., Bonilla 1982). The lack of Raman bands in Co- and Ni-olivines is chiefly attributed to weak intensity of signals. It should be noted that different assignments of Raman modes for olivine exist in the literature. For example, the Raman band of forsterite at 375 cm^{-1} (corresponding to the bands at 328 and 344 cm^{-1} in Co- and Ni-olivines, respectively, see Table 1) was also assigned to be a mix (Mg, T) (a lattice mode, Chopelas 1991), while the two strongest Raman bands at 825 and 856 cm^{-1} in forsterite may be the mixtures of v_1 and v_3

Fig. 1a, b The ambient Raman spectra of **a** Co-olivine and **b** Ni-olivine. Note that the full scale of intensity in **a** is only one tenth of that in **b**
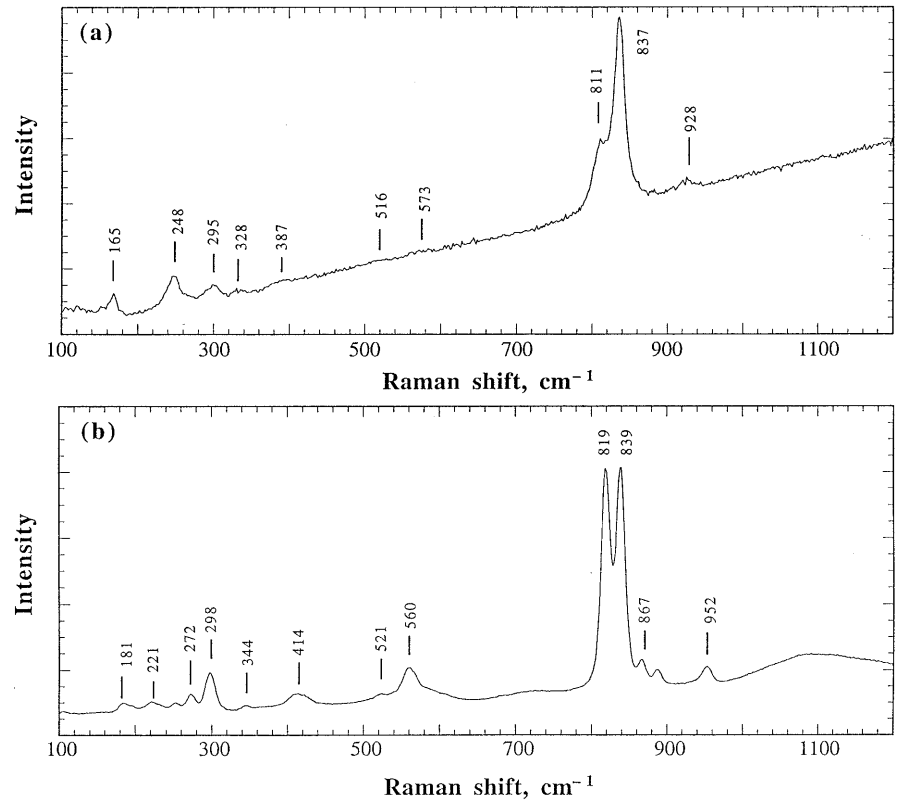

Table 1 Ambient frequencies (cm^{-1}) of Raman modes of forsterite (Mg$_2$SiO$_4$), Co-, and Ni- (liebenbergite) olivines and their symmetries and assignments[a]

Symmetries and assignments[b]	Forsterite	Co-olivine	Ni-olivine
A_g T(M$_2$, SiO$_4$:x)	183	135 ± 4 w	
B_{1g} T(SiO$_4$, M$_2$:y)	192	165 ± 2 w	181 ± 1 w
A_g T(SiO$_4$, M$_2$:y)	226 ± 2		191 ± 2 w
B_{2g} T(SiO$_4$:z)	243 ± 1		221 ± 3 w
A_g T(M$_2$, SiO$_4$:x)	305 ± 2	248 ± 2 w	252 ± 2 w
B_{2g} R(SiO$_4$:x)	324 ± 2		272 ± 2w
A_g T(M$_2$:y)	330 ± 1		298 ± 2 m
B_{2g} R(SiO$_4$:y)	366 ± 3	295 vw	
B_{3g} R(SiO$_4$:z)	375 ± 1	328 w	344 ± 2 w
B_{1g} T(M$_2$)[c]	383	336 vw	
B_{1g} v_2	435 ± 3	387 mw	414 ± 1 m
A_g v_4	546 ± 2	516 ± 1 mw	521 ± 2 mw
B_{3g} v_4	593 ± 3	552 ± 3 mw	560 ± 1 ms
B_{1g} v_4	632	573 vw sh	593 ± 3 w sh
A_g v_1	825 ± 1	811 ± 1 s	819 ± 1 vs
A_g v_3	856 ± 1	837 ± 1 vs	839 ± 1 vs
B_{2g} v_3	882 ± 3		868 ± 2 m sh
B_{3g} v_3	921 ± 1	885 ± 3 mw	889 ± 3 m
A_g v_3	966 ± 2	928 ± 4 m	952 ± 2 m

[a] Data of synthetic forsterite are the average of those reported in literature, and both data of Co- and Ni-olivines are from this work. *vs* very strong; *s* strong; *ms* medium to strong; *m* medium; *mw* weak to medium; *w* weak; *vw* very weak; *sh* should
[b] The symmetries and assignments are based on those for forsterite (Iishi 1978). *T* translation; *R* rotation of SiO$_4$; M_2 MgO$_6$ at M$_2$ site; v_1 symmetric stretching; v_2 symmetric deformation; v_3 asymmetric stretching; v_4 asymmetric deformation
[c] Assignment of Chopelas (1991)

(Wang et al. 1993) or v_3 for the 825 cm^{-1} band and v_1 or v_2 for the 856 cm^{-1} band (Chopelas 1991; Mohanan et al. 1993).

Under ambient conditions, the Raman intensity in Ni-olivine is 1 order of magnitude stronger than that in Co-olivine (Fig. 1), though the crystal size of the latter (ca. 100–200 μm) is far larger than that of the former (< 30 μm). The far weaker Raman intensity in Co-olivine has been attributed to smaller electronegativity and larger average atomic weight in cobalt (Lin 2001).

Quasihydrostatic compression

The pressure variation of Raman frequencies of the two olivines was studied up to 30–35 GPa at room temperature. The mode frequencies as a function of pressure are shown in Figs. 2 and 3 for Co- and Ni-olivines, respectively. To discriminate one mode from others, several symbols are used in these figures. The solid lines (curves) are the regression lines (curves), while dashed lines are used for linear extrapolation and the highly uncertain data sets. For the sake of comparison, the frequency–pressure plots (v–P plots) obtained under both quasi- and nonhydrostatic conditions for the same sample are shown in the same figure. The ambient frequencies (v_i) and the regression constants are listed in Tables 2 and 3 for Co- and Ni-olivines, respectively. Note that the scattering of data in Figs. 2 and 3 at higher pressure is chiefly attributed to weak intensity and significant overlap of bands, which resulted in larger error in estimation of the peak position.

It should be noted that many Raman frequencies of the two olivines show a significant shift between atmospheric pressure and 0.3 GPa (1–3 kbar). This phenomenon has not been reported for other olivines before. However, a similar case in hydroxyl-chondrodite has been observed (Lin et al. 1999). The reason for the significant frequency increase at low pressure is not clear, though it may involve a slight distortion of the crystal lattice, like that suggested for chondrodite. The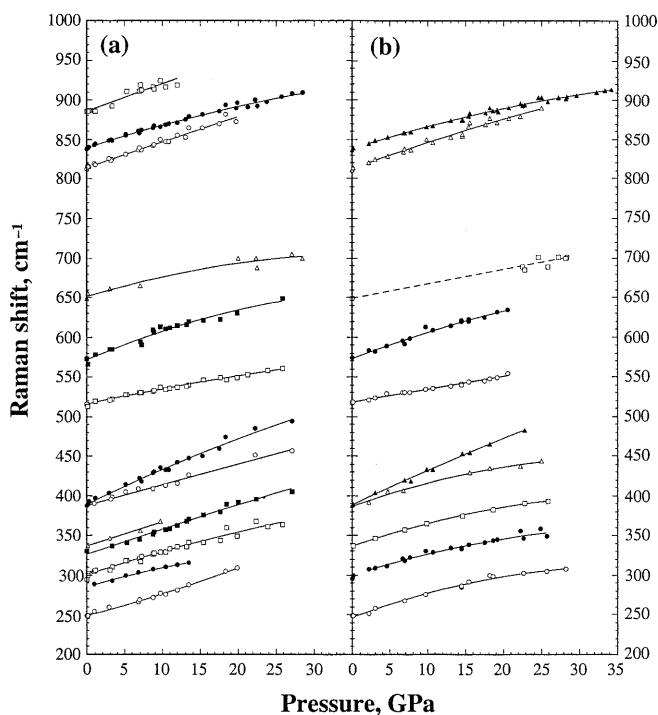refore, the data obtained below 0.3 GPa for these bands were excluded from the fitting process of the v–P plots. Some of the regression constants in Table 2 and all constants in Table 3 were obtained on the basis of the data above 0.3 GPa.

Pressure dependence of Raman spectra

Figures 2a and 3a display the pressure dependences of the Raman frequencies obtained under quasihydrostatic condition for Co- and Ni-olivines, respectively. All of the Raman frequencies increase with increasing pressure. As some Raman modes observed in forsterite (e.g., Besson et al. 1982; Chopelas 1990; Durben et al. 1993; Liu and Mernagh 1993; Wang et al. 1993), most of the v–P plots for both Co- and Ni-olivines are nonlinear. For forsterite, the nonlinear v–P plots has been considered to be caused by a second-order phase transition (Chopelas 1990) or a change in compression mechanism (Wang et al. 1993). However, Liu and Mernagh (1993) did not agree with these viewpoints. The X-ray diffraction studies also did not reveal a discontinuity in forsterite up to 40 GPa (e.g., Will et al. 1986; Andrault et al. 1995; Zhang 1998). The loss of hydrostaticity at high pressures may contribute to the nonlinearity of a v–P plot. However, on the basis of the definitions of mode Grüneisen parameter and isothermal bulk modulus of a substance, it has been pointed out that a non-

Fig. 2a, b Pressure dependences of the Raman bands of Co-olivine under **a** quasihydrostatic and **b** nonhydrostatic conditions and at room temperature
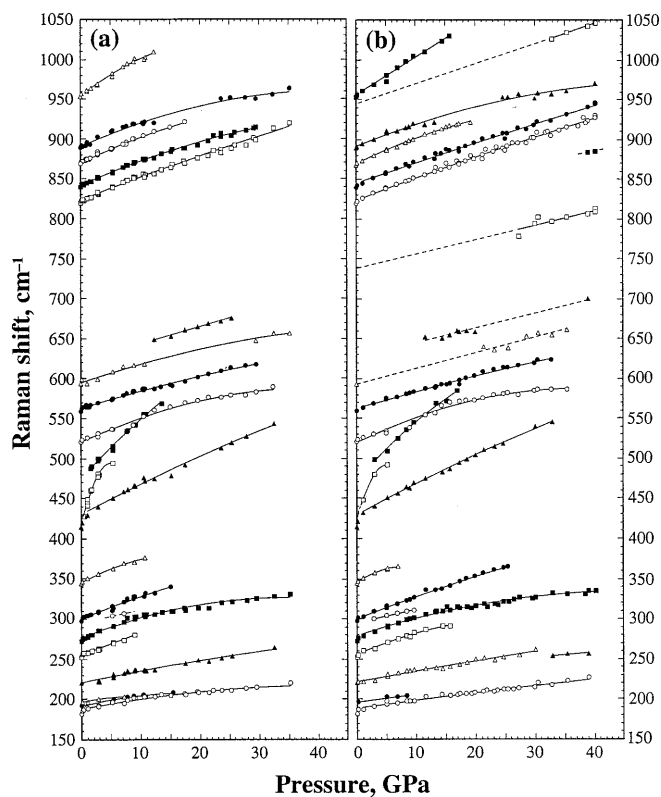

Fig. 3a, b Pressure dependences of the Raman bands of Ni-olivine under **a** quasihydrostatic and **b** nonhydrostatic conditions and at room temperature

Table 2 Regression constants of Co-olivine for Raman bands determined in $\Delta v = v_0 + aP + bP^2$ at room temperature. v_i, v_0 and Δv are in cm^{-1}, P in GPa, and the constants, a and b have the corresponding units. v_i is the frequency measured at ambient conditions. R is the correlation coefficient

v_i	Quasihydrostatic				Nonhydrostatic			
	v_0	a	$b \times 10^2$	R	v_0	a	$b \times 10^2$	R
248	248.8	2.33	3.39	0.997	246.4	3.52	−4.78	0.996
	285.2	2.78	−4.08	0.997				
295[a]	300.7	3.06	−2.03	0.983	300.0	2.97	−3.50	0.980
328	326.0	3.18	−0.42	0.992				
336	336.1	3.0		0.994	336.3	3.25	−4.01	0.999
387	387.4	2.62		0.993	386.3	3.43	−4.74	0.996
387	389.0	4.63	−2.51	0.995	388.1	4.52	−1.61	0.998
516	515.9	2.00	−1.15	0.994	517.6	1.62		0.993
573	571.6	4.02	−4.53	0.982	572.5	3.65	−3.33	0.991
649	651.3	2.8	−3.5	0.976	648.5	1.8		0.993
811[a]	813.4	3.29	−0.23	0.986	812.3	3.51	−1.83	0.986
837[a]	839.3	2.97	−1.88	0.994	837.8	3.03	−2.43	0.994
885	885.5	3.4		0.955				

[a] Data obtained under $P < 0.3$ GPa were excluded from regressions

Table 3 Regression constants of Ni-olivine for Raman bands determined in $\Delta v = v_0 + aP + bP^2$ at room temperature. v_i, v_0, and Δv are in cm^{-1}, P in GPa, and the constants, a and b have the corresponding units. v_i is the frequency measured at ambient conditions. R is the correlation coefficient. The regression constants were based on the data obtained from $P > 0.3$ GPa

v_i	Quasihydrostatic				Nonhydrostatic			
	v_0	a	$b \times 10^2$	R	v_0	a	$b \times 10^2$	R
181	187.6	1.37	−1.57	0.984	188.2	1.02	−0.26	0.989
191	191.1	1.8	−5.0	0.999				
	195.8	1.8	−10.4	0.986				
221	220.8	1.50	−0.71	0.980	221.5	1.36	−0.32	0.990
252	255.5	2.76		0.993	253.4	3.25	−5.81	0.992
272	277.0	2.82	−4.00	0.990	279.6	2.38	−2.59	0.990
298	300.5	2.96	−2.29	0.989	299.7	2.89	−1.22	0.998
(298?)					295.1	1.57		0.997
344	345.5	4.03	−11.19	0.995	345.6	4.97	−31.18	0.996
	417.7	30.61	−306.9	0.996				
414	429.8	3.95	−1.57	0.995	429.1	3.99	−1.34	0.999
	475.7	7.97	−6.43	0.996	472.3	8.46	−11.16	0.997
521	520.4	3.42	−4.26	0.995	518.9	3.68	−4.94	0.990
560	563.5	2.17	−1.05	0.996	562.0	2.21	−0.84	0.995
593	594.2	2.55	−2.27	0.994	593.1	2.0		0.986
	622.7	2.08		0.994	626.6	1.9		0.986
					737.4	1.82		0.880
819	823.5	2.82	−0.64	0.996	823.8	2.77	−0.55	0.996
839	841.6	3.24	−2.80	0.998	844.6	2.55	−0.29	0.997
868	869.5	3.54	−3.94	0.996	869.2	3.64	−4.50	0.998
889	889.7	3.30	−3.82	0.994	890.9	3.03	−2.78	0.994
					944.5	2.5		0.995
952	954.0	5.82	−11.78	0.994	953.9	5.30	−3.14	0.992

linear v–P plot is not an abnormal case if a change in crystal structure is not accompanied throughout a wide pressure range (Liu and Wu 1992; Lin et al. 2000). The v–P plots in Figs. 2a and 3a are continuous throughout the whole pressure range studied. Therefore, we observed no evidence that a phase transition or change in compression mechanism has taken place in Co- and Ni-olivines at room temperature and below 30 GPa.

Under compression, the ambient band of Co-olivine at 387 cm^{-1} split into two peaks (Fig. 2a), indicating that this band may be a doubly degenerate mode or a mixture of two modes. This band corresponds to the ambient band of forsterite at 435 cm^{-1}, which is considered to be a single mode (Iishi 1978; Bonilla 1982) or

a mixture of v_2 and a rotation mode of SiO$_4$ (Chopelas 1990). The group analysis does not predict the E_g mode in olivine. Hence, Chopelas's assignment (1990) may be correct. On the other hand, the two strongest modes of Co-olivine (the ambient bands at 811 and 837 cm^{-1}) gradually approach each other under compression (Fig. 2a) and, finally, only the higher-frequency mode can be recognized at pressures above 20 GPa. This case indicates that the vibration corresponding to the ambient 811 cm^{-1} band should have a stronger pressure effect than the 837 cm^{-1} band on its polarizability and thus Raman intensity.

Relative to Co-olivine, the Raman spectra of Ni-olivine are somewhat complicated. This is due to stronger

Table 4 Ambient frequencies and pressure derivatives (*values in parentheses*) of the lattice and internal modes for forsterite, Co- and Ni-olivines at 1 GPa (quasihydrostatic, P in GPa and frequency in cm^{-1})[a]

Modes and assignments	Forsterite (α-Mg$_2$SiO$_4$)					α-Co$_2$SiO$_4$	α-Ni$_2$SiO$_4$
	Ambient	a	b	c	d		
A_g T(M$_2$, SiO$_4$:x)	183	(3.03)	(3.01)				
B_{1g} T(SiO$_4$, M$_2$:y)	192						181 (1.34)+
A_g T(SiO$_4$, M$_2$:y)	226 ± 2	(1.20)	(1.22)				191 (1.69)+
B_{2g} T(SiO$_4$:z)	243 ± 1	(2.30)	(2.35)				221 (1.48)+
B_{3g} T(M$_2$)[b]	288 ± 2		(3.06)				
A_g T(M$_2$, SiO$_4$:x)	305 ± 2	(3.90)	(3.86)			248 (2.39)+	252 (2.76)
B_{2g}[c]	324 ± 1						272 (2.74)+
A_g T(M$_2$:y)	330 ± 1	(3.00)	(2.95)			283 (2.70)+	298 (2.92)+
A_g[c]	340 ± 2	(4.98)	(4.63)				
B_{3g}[c]	375 ± 1	(3.68)					344 (3.80)+
B_{1g} T(M$_2$)[d]	383					336 (3.03)	
Average (lattice modes)		(3.16)	(3.01)			(2.7)	(2.39)
B_{3g} v_2	411 ± 1	(3.18)	(3.12)				
A_g v_2	424 ± 2	(4.75)	(4.80)				
B_{1g} v_2	435 ± 3	(4.74)	(4.58)	(5.97)+		387 (2.62)+	414 (3.91)+
B_{2g} v_2	441 ± 1	(5.50)	(5.45)				
A_g v_4	546 ± 2	(2.25)	(1.95)			516 (1.97)+	521 (3.34)+
B_{1g} v_4	584 ± 2	(3.00)	(2.18)				
B_{2g} v_4	589 ± 4		(2.80)				
B_{3g} v_4	593 ± 2						560 (2.15)+
A_g v_4	609 ± 1	(3.35)	(3.24)	(3.20)+	(3.0)		
B_{1g} v_4	632					573 (3.93)+	593 (2.51)+
A_g v_1	825 ± 1	(3.12)	(3.07)	(3.38)+	(3.44)+	811 (3.28)+	819 (2.81)+
B_{1g} v_1	838 ± 1			(3.67)+			
A_g v_3	856 ± 1	(3.27)	(3.09)	(3.59)+	(3.4)	837 (2.93)+	839 (3.19)+
B_{1g} v_3	865 ± 1			(3.79)+			
B_{2g} v_3	882 ± 3	(3.03)	(3.03)	(3.71)+			868 (3.46)+
B_{3g} v_3	921 ± 1	(2.75)	(2.76)		(3.9)	885 (3.4)	889 (3.23)+
A_g v_3	966 ± 2	(5.01)	(5.01)	(6.84)+			952 (5.59)+
Average (internal modes)		(3.66)	(3.47)	(4.27)	(3.44)	(3.02)	(3.35)

[a] The ambient frequencies of forsterite are the average of those reported in literature. Except the bands corresponding to the 288 cm^{-1} and 383 cm^{-1} bands of forsterite, the assignments are based on those reported by Iishi (1978). Data of forsterite are cited from a Chopelas (1990), b Wang et al. (1993), c Liu and Mernagh (1993), and d Besson et al. (1982). Data of Co- and Ni-olivines are from this work

[b] Assignment of Wang et al. (1993)

[c] According to Chopelas (1991), these modes are the lattice modes

[d] Assignments of Chopelas (1991)

+ Values were obtained from the quadratic-polynomial pressure–frequency plots

signals in Ni-olivine. Three weak bands were observed in the range of 180–210 cm^{-1}. Similarly to the 387 cm^{-1} band of Co-olivine, the ambient band of Ni-olivine at 414 cm^{-1} also splits into two bands under compression (Fig. 3a). However, unlike Co-olivine, the new band ($v_0 = 417.7$ cm^{-1} in Table 3) showed rather steep pressure dependence. Besides, another new band ($v_0 = 475.7$ cm^{-1}, which also has a steep v–P slope) appeared at pressures above 1.5 GPa, and intensity of this band increases with increasing pressure up to 10.5 GPa. The large v–P slope may involve significant distortion of SiO$_4$ under compression if these vibrations are asymmetric internal modes. However, the Ni-olivine specimens used in this work contain some unreacted cristobalite (SiO$_2$). Therefore, the two new bands may be bands of cristobalite (adhered on the olivine crystals) with the ambient frequencies of 417 and 466 cm^{-1}.

The two strongest Raman bands in Ni-olivine (the ambient bands at 819 and 839 cm^{-1}) also gradually approach each other under compression (Fig. 2a), but only the lower frequency mode can be recognized at pressures above 30 GPa. This case is opposite to that observed in Co-olivine. The two olivines have the same crystal structure and vibrations. Hence, the different pressure dependences of polarizability (or Raman intensity) for the same A_g internal modes may suggest that the two strongest signals in Co- and Ni-olivines are the mixtures of v_1 and v_3 (with different v_1/v_3 ratio for the two olivines) as proposed by Chopelas (1991) and Wang et al. (1993), not the pure v_1, v_2, or v_3 assigned by other authors (Iishi 1978; Chopelas 1990; Mohanan et al. 1993).

Compressional behavior of polyhedra

As mentioned previously, a significant shift in frequency has been found in many Raman bands of Co- and Ni-olivines. Therefore, the v–P slopes at 1 GPa were chosen for comparison. Table 4 lists the pressure derivatives

(dv/dP) of all lattice and internal modes obtained at one GPa and room temperature for forsterite, Co- and Ni-olivines. The data for forsterite were also extracted from synthetic crystals. Except for the data noted by the plus (+) symbol, all the pressure derivatives in Table 4 were obtained from linear regressions of the v–P plots. It should be noted that the discrimination of lattice modes from internal modes of SiO_4 is only a convention. Actually, neither a pure lattice mode nor a pure internal SiO_4 mode can be found in a crystal.

At one GPa, the average dv/dP of the lattice Raman modes in forsterite, Co- and Ni-olivines is smaller than that of the SiO_4-internal modes (see Table 4). The difference in the average dv/dP between the two groups of modes is 0.3–1.0, which is large and cannot be simply regarded as experimental uncertainty. The same relationship for the average dv/dP of the two groups of modes is also found in the two olivines and forsterite at other pressures, though the data of the latter (see Table 4) were obtained from the static compression runs using different pressure media. It should be noted that the loss of hydrostaticity at higher pressure may result in a change in the pressure dependences. However, in the present experiments, the system is nearly hydrostatic below 10 GPa. Therefore, the larger average dv/dP observed in the internal modes at 1 GPa is indeed the property of these olivines.

If the decrease in unit-cell volume and the shortening of chemical bonds are the determining factors for the increase of Raman frequencies under compression, one can conclude that the SiO_4 tetrahedra in the three olivines (Mg, Co, Ni) are more compressible than the cation octahedra. However, this conclusion is contrary to the result of X-ray diffraction of forsterite (Hazen 1976, 1977). Hazen's studies indicate that the octahedra in an olivine are more compressible than the SiO_4 tetrahedra. Supposing that the conclusion extracted from the diffraction data of forsterite can be applied to the case of Co- and Ni-olivines, then the larger average dv/dP for the internal modes should reveal that the SiO_4 tetrahedra in the three olivines have received more significant distortion (e.g., nonideal bond angles) than the octahedra received under compression. The larger increase in strain energy of the SiO_4 tetrahedra may result in faster change in vibrational frequency. This argument is consistent with the results reported by Hazen (1976), in which the distortion of SiO_4 tetrahedra increases with increasing pressure, but little change in octahedra.

On the basis of X-ray diffraction data (Hazen 1976, 1977), the lattice modes should be the best set of vibrational modes for observing the effects of CFSE and cation size on the compressional behavior of olivines. Unfortunately, all the dv/dP data of the lattice modes and most of the internal modes of tephroite and fayalite are unavailable at present. Thus, a clear picture of the effect of transition metal cations on the compressional behavior of polyhedra in various silicate olivines cannot be obtained yet.

Nonhydrostatic compression

The pressure dependences of Raman frequencies for both Co- and Ni-olivines under nonhydrostatic condition are given in Figs. 2b and 3b. Similarly to that observed in quasihydrostatic experiments, many Raman modes display a significant frequency shift between atmospheric pressure and 0.3 GPa. Therefore, the regression constants of the v–P plots were also obtained from the data above 0.3 GPa.

For nonhydrostatic compression of the two olivines, the average dv/dP of the lattice modes is also smaller than that of the internal modes of SiO_4, but the difference between the two groups of modes is slightly smaller than that obtained under quasihydrostatic condition. The difference in the v–P trajectories obtained under both quasi- and nonhydrostatic experiments is small, especially at lower pressures (e.g., Fig 2a, b). This result indicates that the effect of shear stress on the vibrations of the chemical bonds in olivines may be rather minor, or the stress deviator developed around the measured points of the samples under the present nonhydrostatic condition was not large enough. The negligible effect of shear stress on the pressure dependences of Raman frequencies has been also observed in forsterite (Sharma et al. 1992), the low-frequency ($< 1200 \, cm^{-1}$) Raman bands of hydroxyl-clinohumite (Lin et al. 2000), and superhydrous phase B.

For Co-olivine, the Raman spectra obtained under both quasi- and nonhydrostatic experiments are similar. However, there are four new bands appearing in the Raman spectra of Ni-olivine at pressures above 30 GPa, but no change in color of sample was observed. These new bands are neither the Raman bands of Ni-olivine nor the bands of NiO, SiO_2, and their high-pressure phases. Figure 4 shows the representative Raman spectra of Ni-olivine as a function of nonhydrostatic pressure at room temperature. Extrapolating the two most reliable new bands to zero pressure has obtained the zero-pressure frequencies (v_0) of 737 and 944 cm^{-1} (Table 3). The v_0 from linear extrapolation of the other two new weak bands are $\sim$235 and $\sim$843 cm^{-1}. A similar case has been observed in forsterite at pressures above 30 GPa and room temperature (Durben et al. 1993). However, the bands corresponding to the v_0 of $\sim$235 and $\sim$843 cm^{-1} in Ni-olivine were not observed in forsterite.

The frequencies of all Raman modes of Ni-olivine are lower than those of the corresponding modes of forsterite (Table 1). Thus, the Raman frequencies of the high-pressure phases of Ni-olivine, if any, should be lower than those of the corresponding high-pressure phases of forsterite. Using this criterion, the new bands appearing in the Raman spectra of Ni-olivine above 30 GPa are not the Raman bands of modified spinel (β-phase), spinel (γ-phase), perovskite, ilmenite, and majorite phases (Liu et al. 1994). Durben et al. (1993) attributed the two new bands in forsterite to the formation of high-pressure defects, e.g., Si–O–Si dimer linkages, via polymerization of adjacent SiO_4 tetrahedra. They also suggested that the
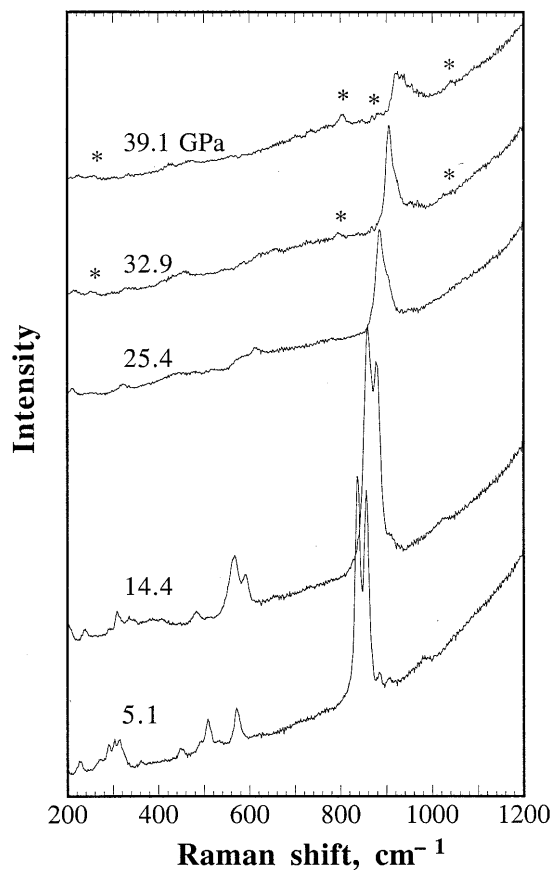
Fig. 4 Selected Raman spectra of Ni-olivine as function of (nonhydrostatic) pressure at room temperature. The *asterisks* indicate the new bands which appear at a pressure above 30 GPa

formation of dimer defects in olivine may or may not be accompanied by an increase in coordination of Si, and is a prelude to irreversible amorphization at higher pressures.

The criteria for pressure-induced amorphization of a compound are: (1) the compound has a high-pressure polymorph, but the formation of the high-pressure phase is hindered kinetically at the concerned temperature and (2) the extrapolation of the melting curve to the P–T stability field of the high-pressure phase has a negative slope (Brazhkin and Lyapin 1996; Richet and Gillet 1997). It is known that forsterite, fayalite, Co-olivine, and Ni-olivine have the same type of high-pressure phase (the γ-phase; Liu and Bassett 1986). Therefore, according to Durben et al. (1993), Ni-olivine may become amorphous at still higher pressure ($P > 40$ GPa), though we do not know if the P–T slope of the extending melting curve is negative.

It should be noted that the experiment of Durben et al. (1993) was carried out at room temperature, like this work, a condition different from that for amorphization of forsterite (< 700 °C and 30 GPa, see Guyot and Reynard 1992). Besides, a total of four new Raman bands were observed in Ni-olivine. Therefore, the appearance of the new bands above 30 GPa may not be the

prelude to amorphization of olivine. Instead, the formation of a new high-pressure phase is possible. Recently, a study using X-ray diffraction at room temperature has pointed out that forsterite gradually becomes amorphous under compression, and a few weak Bragg reflections were observed at pressures above 35 GPa (Andrault et al. 1995). The appearance of these reflections may indicate the formation of β-phase or of an intermediate spinelloid phase (Andrault et al. 1995). To clarify this point, a comparative in situ high-pressure study on olivine and β-phase using both Raman and X-ray diffraction should be carried out in the future.

References

Andrault D, Bouhifd MA, Itié JP, Richet P (1995) Compression and amorphization of $(Mg,Fe)_2SiO_4$ olivines: an X-ray diffraction study up to 70 Gpa. Phys Chem Miner 22: 99–107

Besson JM, Pinceaux JP, Anastopoulos C, Velde B (1982) Raman spectra of olivine up to 65 kilobars. J Geophys Res 87(B): 10773–10775

Bonilla IR (1982) Raman spectra of forsterite. J Quant Spectrosc Radiat Transfer 38: 527–529

Brazhkin VV, Lyapin AG (1996) Lattice instability approach to the problem of high-pressure solid-state amorphization. High Press Res 15: 9–30

Brown Jr GE (1982) Olivines and silicate spinels. In: Ribbe PH (ed) Orthosilicates. Mineralogical Society of America, Washington DC, pp 275–381

Chopelas A (1990) Thermal properties of forsterite at mantle pressures derived from vibrational spectroscopy. Phys Chem Miner 17: 149–156

Chopelas A (1991) Single-crystal Raman spectra of forsterite, fayalite, and monticellite. Am Mineral 76: 1101–1109

Deer WA, Howie RA, Zussman J (1992) An introduction to the rock-forming minerals. Longman Sci. & Tech., Essex, pp 3–13

Downs RT, Zha C-S, Duffy TS, Finger LW (1996) The equation of state of forsterite to 17.2 GPa and effects of pressure media. Am Mineral 81: 51–55

Durben DJ, McMillan PF, Wolf GH (1993) Raman study of the high-pressure behavior of forsterite (Mg_2SiO_4) crystal and glass. Am Mineral 78: 1143–1148

Guyot F, Reynard B (1992) Pressure-induced structural modifications and amorphization in olivine compounds. Chem Geol 96: 411–420

Hazen RM (1976) Effects of temperature and pressure on the crystal structure of forsterite. Am Mineral 61: 1280–1293

Hazen RM (1977) Effects of temperature and pressure on the crystal structure of ferromagnesian olivine. Am Mineral 62: 286–295

Iishi K (1978) Lattice dynamics of forsterite. Am Mineral 63: 1198–1208

Jeanloz R, Lally JS, Nord Jr GL, Christie JM, Heuer AH (1977) Shock-produced olivine glass: first observation. Science 197: 457–458

Lin CC (2001) Vibrational spectroscopic study of the system α-Co_2SiO_4–α-Ni_2SiO_4. J Sol State Chem (in press)

Lin CC, Liu L, Irifune T (1999) High-pressure Raman spectroscopic study of chondrodite. Phys Chem Miner 26: 226–233

Lin CC, Liu L, Mernagh TP, Irifune T (2000) Raman spectroscopic study of hydroxyl-clinohumite at various pressures and temperatures. Phys Chem Miner 27: 320–331

Liu L, Bassett WA (1986) Elements, oxides, and silicates: high-pressure phases with implications for the Earth's interior. Oxford University Press, New York, pp 211–219

Liu L, Mernagh TP (1993) Raman spectra of forsterite and fayalite at high pressures and room temperature. High Press Res 11: 241–256

Liu L, Wu L (1992) Bulk modulus and equation of state. Phys Earth Planet Inter 70: 78–84

Liu L, Mernagh TP, Irifune T (1994) High pressure Raman spectra of β-Mg_2SiO_4, γ-Mg_2SiO_4, $MgSiO_3$-ilmenite and $MgSiO_3$-perovskite. J Phys Chem Sol 55: 185–193

Matsui Y, Syono Y (1968) Unit-cell dimensions of some synthetic olivine group solid solutions. Geochem J 2: 51–59

Mohanan K, Sharma SK, Bishop FC (1993) A Raman spectral study of forsterite-monticellite solid solutions. Am Mineral 78: 42–48

Morimoto N, Tokonami M, Watanabe M, Koto K (1974) Crystal structures of three polymorphs of Co_2SiO_4. Am Mineral 59: 475–485

Reynard B, Remy C, Takir F (1997) High-pressure Raman spectroscopic study of Mn_2GeO_4, Ca_2GeO_4, Ca_2SiO_4, and $CaMgGeO_4$ olivines. Phys Chem Miner 24: 77–84

Richard G, Richet P (1990) Room-temperature amorphization of fayalite and high-pressure properties of Fe_2SiO_4 liquid. Geophys Res Lett 17: 2093–2096

Richet P, Gillet P (1997) Pressure-induced amorphization of minerals: a review. Eur J Mineral 9: 907–933

Sharma SK, Cooney TF, Wang SY (1992) Effect of high P and high T on olivines – a Raman spectral study. In: Singh AK (ed) Recent trends in high-pressure research. Oxford & IBH, New Delhi, pp 614–619

Syono Y, Tokonami M, Matsui Y (1971) Crystal field effect on the olivine-spinel transformation. Phys Earth Planet Inter 4: 347–352

Wang SY, Cooney TF, Sharma SK (1992) Infrared studies of glasses and crystals of olivine composition at high pressures. In: Singh AK (ed) Recent trends in high-pressure research. Oxford & IBH, New Delhi, pp 611–613

Wang SY, Sharma SK, Cooney TF (1993) Micro-Raman and infrared spectral study of forsterite under high pressure. Am Mineral 78: 469–476

Will G, Hoffbauer W, Hinze E, Lauterjung J (1986) The compressibility of forsterite up to 300 kbar measured with synchrotron radiation. Physica 139/140(B): 193–197

Williams Q, Knittle E, Reichlin R, Martin S, Jeanloz R (1990) Structural and electronic properties of Fe_2SiO_4-fayalite at ultrahigh pressure: amorphization and gap closure. J Geophys Res 95(B): 21549–21563

Zhang L (1998) Single crystal hydrostatic compression of $(Mg,Mn,Fe,Co)_2SiO_4$ olivines. Phys Chem Miner 25: 308–312